Islamic University Journal of Applied Sciences (IUJAS)
https://journals.iu.edu.sa/jesc

Volume VIII, Issue II, December 2026, Pages 202-216

Non-Isothermal Melting Kinetics of Pb-61.9Sn-2Al Eutectic-Based Alloy: A Differential Thermal Analysis Study

Ali Alnakhlani [1] *

[1] Department of Physics, College of Science, Qassim University, Buraydah 51452, Saudi Arabia

*Corresponding author, *E-mail addresses*: A.Alnakhlany@qu.edu.sa

Abstract

The non-isothermal melting kinetics of a Pb–61.9 wt% Sn–2 wt% Al ternary alloy were investigated by differential thermal analysis (DTA) at five constant heating rates (β = 10, 15, 20, 25 and 30 °C min^{-1}). A 40 mg specimen was scanned from ambient to 400 °C under inert atmosphere using α-Al_2O_3 as the reference material. The melting onset (184.5–190.9 °C) remained in close agreement with the canonical Pb-Sn eutectic of 183 °C, confirming that the 2 wt% Al microaddition does not displace the eutectic temperature. Three complementary model-free kinetic treatments — Kissinger, Ozawa–Flynn–Wall (OFW) and Augis–Bennett — were applied to the main endotherm. The Kissinger and OFW methods yielded mutually consistent apparent activation energies of 138.63 and 139.35 kJ mol^{-1} (R^2 = 0.989 and 0.990) with a relative deviation ≈ 0.5 %,consistent with the fact that these two model-free treatments are near-identical transforms of the same (β, T_p) dataset; their close agreement therefore reflects internal arithmetic consistency rather than independent cross-validation. The Augis–Bennett analysis returned a systematically lower value of 73.63 kJ mol^{-1} (R^2 = 0.891), attributable to its inherent sensitivity to the heating-rate-dependent peak width, which broadened nearly threefold (from 18.04 to 50.67 °C) across the experimental range; this broadening is the distinctive thermal signature of the dispersed insoluble Al-rich grains introduced by the microaddition.

Keywords: Differential thermal analysis; Pb-Sn-Al alloy; Eutectic melting; non-isothermal kinetics; Activation energy; Kissinger method; Ozawa-Flynn-Wall; Augis-Bennett.

https://doi.org/10.63070/jesc.2026.040
Received 14 April 2026; Revised 28 May 2026; Accepted 13 June 2026; Available online 20 June 2026.
Published by Islamic University of Madinah on behalf of ***Islamic University Journal of Applied Sciences.***
This is an open access article published under the Creative Commons Attribution 4.0 International license (CC BY 4.0):https://creativecommons.org/licenses/by/4.0/

1. Introduction

Tin–lead solders have served as the cornerstone of metallurgical joining in microelectronics for more than a century, owing to their low melting temperatures, favourable wetting characteristics, and reproducible mechanical behaviour [1,2]. Although global legislative drivers have promoted lead-free formulations across consumer electronics over the past two decades [3–5], Pb-Sn solders remain essential in high-reliability sectors such as aerospace, defence, medical implants, and high-temperature power electronics, where qualified Pb-free substitutes are still under development [6,7]. The eutectic Pb-Sn composition (Sn-61.9 wt% / Pb-38.1 wt%) melts congruently at 183 °C and remains the reference benchmark against which all candidate joining alloys are compared [1,8,9]. Beyond binary Pb-Sn formulations, ternary modifications have attracted continuous interest because minor element additions can refine the solidification microstructure, alter the intermetallic-phase distribution, and tune the mechanical response without dramatically shifting the eutectic temperature [3,8]. Aluminium, in particular, exhibits very limited solid solubility in both lead and tin under near-equilibrium conditions [2], so that small Al additions to a near-eutectic Pb-Sn matrix form dispersions of primary Al-rich grains rather than a ternary solid solution. The mechanical and thermal consequences of such Al microadditions have, however, received comparatively little systematic attention in the open literature, and the corresponding melting kinetics, essential for accurate process modelling of reflow and joining cycles remain largely uncharacterised. Differential thermal analysis (DTA) and differential scanning calorimetry (DSC) are the established techniques for resolving solid–liquid phase transitions in metallic systems, providing direct access to the characteristic temperatures (onset, peak, end) and to the enthalpy associated with the transformation [9,10]. When DTA is performed at multiple constant heating rates, the peak temperature T_p of the melting event shifts to higher values with increasing heating rate β. This heating-rate dependence encodes the apparent activation energy of the underlying kinetic process, and three classical non-isothermal methods proposed independently by Kissinger [11], Ozawa [12], Flynn and Wall [13], and Augis and Bennett [14] exploit this shift to extract the apparent activation energy Ea without an a priori model of the reaction mechanism. These methods, originally developed for crystallisation and solid-state reaction kinetics [15–19], have since been extended to melting phenomena, polymer degradation, and glass transitions [20–22]. Applying more than one formulation provides a useful consistency check on the extracted E_a; it should be noted, however, that the Kissinger and OFW expressions are near-identical transforms of the same (β, T_p) data and therefore do not constitute independent cross-validation, whereas the Augis–Bennett treatment differs through its normalisation by the onset-to-peak interval [21–24].The recent critical review by Vyazovkin [24] emphasises that even when the Kissinger plot appears highly linear the underlying assumption of single-step first-order kinetics may mask additional complexity; consequently, the joint deployment of

complementary methods is now considered essential good practice. In the present study, a Pb-61.9Sn-2Al ternary alloy was investigated by DTA at five heating rates (β = 10, 15, 20, 25, and 30 °C min^{-1}) using a 40 mg specimen scanned from ambient (room temperature) to 400 °C. The principal objectives were: (i) to map the thermal signature of the alloy and identify all thermal events occurring within this temperature window; (ii) to extract the characteristic temperatures and enthalpy of the eutectic melting event; (iii) to determine the apparent activation energy of the melting transformation by the Kissinger, Ozawa-Flynn-Wall, and Augis-Bennett formulations and to compare these values critically; and (iv) to discuss the implications of the Al microaddition for the kinetics and morphology of the eutectic transformation. The results provide a quantitative kinetic and thermophysical database for Pb-Sn-Al solders that can inform reflow-profile design and serve as a baseline for further compositional optimisation.

2. Theoretical framework

Non-isothermal kinetic analysis rests on the general rate equation

$$\frac{d\alpha}{dt} = A \cdot exp\left(-\frac{E_a}{RT}\right) \cdot f(\alpha) \qquad (1)$$

where α is the conversion fraction, A the pre-exponential factor, R the universal gas constant, T the absolute temperature, and f(α) the reaction model. Under a constant heating rate β = dT/dt, eq. (1) becomes:

$$\frac{d\alpha}{dT} = \frac{A}{\beta} \cdot \exp\left(-\frac{E_a}{RT}\right) \cdot f(\alpha) \quad (2)$$

Three model-free formulations that derive Ea from the heating-rate dependence of the peak temperature Tp are summarised below [11–14]. It should be noted that the Kissinger, OFW, and Augis–Bennett formalisms were originally developed for thermally-activated solid-state and crystallisation kinetics. Eutectic melting is a first-order, thermodynamically-controlled phase transition; the activation energy extracted from the heating-rate dependence of T_p therefore represents an apparent/effective kinetic descriptor ($E_{a,app}$) that encapsulates contributions from heat transfer, thermal lag, and cooperative atomic rearrangement at the solid–liquid interface, rather than a true atomic activation barrier. Vyazovkin [24] has discussed these limitations explicitly and recommends labelling the extracted quantity as an apparent activation energy; this convention is adopted throughout the present work.

2.1 Kissinger Method

Kissinger [11] showed that, at the maximum reaction rate (i.e. at T = Tp), the second derivative $d^2\alpha/dt^2$ vanishes. Combining this condition with eq. (2) for a first-order kinetic process yields

$$\ln\left(\frac{\beta}{T_p^2}\right) = -\frac{E_a}{RT_p} + \ln\left(\frac{AR}{E_a}\right) \quad (3)$$

A plot of $\ln(\beta/T_p^2)$ vs. $1/T_p$ is linear, and its slope ($-E_a/R$) yields the apparent activation energy. Although derived for first-order reactions, the Kissinger equation has been shown to provide reasonably accurate Ea values for a broad range of nucleation-and-growth processes [19,23,24].

2.2 Ozawa-Flynn-Wall (OFW) method

The integral method introduced independently by Ozawa [12] and by Flynn and Wall [13] uses the Doyle approximation [18] of the temperature integral and does not assume a particular form of f(α). It relates the logarithm of the heating rate to the inverse peak temperature:

$$log_{10}\beta = -0.4567 \cdot \frac{E_a}{R\,T_p} + constant \quad (4)$$

The slope of log10 β versus 1/Tp therefore equals −0.4567 E_a/R, yielding $E_a = -R \cdot \text{slope} / 0.4567$. Because the OFW formulation is strictly model-free, it is widely recommended by the ICTAC Kinetics Committee as a cross-check against model-dependent treatments [21,22].

2.3. Augis-Bennett method

Augis and Bennett [14] proposed a modified Kissinger expression that retains the heating-rate dependence but normalises the heating rate by the temperature interval from onset (T_0) to peak (T_p):

$$\ln\left(\frac{\beta}{T_p - T_0}\right) = \ln\left(\frac{AR}{E_a}\right) - \frac{E_a}{RT_p} \quad (5)$$

This formulation has the practical advantage that the intercept directly gives the pre-exponential factor A, and it is particularly suited to transformations with a finite incubation interval. The slope of $\ln[\beta/(T_p - T_0)]$ against $1/T_p$ again yields E_a/R [14,19,23].

3. Experimental Methods

3.1 Alloy Preparation

Two alloy compositions were prepared from elemental Pb, Sn and Al constituents of ≥ 99.99 % purity: a binary Pb–61.9 wt% Sn reference composition and the principal Pb–61.9 wt% Sn–2 wt% Al ternary alloy (61.9 wt% Sn, 2 wt% Al, balance Pb = 36.1 wt%; all components sum to 100 wt%) investigated in detail in this study. Accurately weighed elemental charges were thoroughly mixed in a graphite crucible together with a $CaCl_2$ flux to prevent oxidation during melting. Each melt was cast in a rod geometry using a graphite mould of dimensions 15 × 1 × 1 cm. The as-cast ingots were homogenisation-annealed at 438 K (165 °C) for 50 h, then drawn into wires of 1 mm diameter by cold rolling. Prior to DTA measurements, the wire specimens were re-annealed at 443 K (170 °C) for 4 h and slowly cooled to room temperature at a controlled rate of $\Delta T = 2 \times 10^{-2}$ K s^{-1} to ensure thermodynamic equilibration of the microstructure.

3.2. Differential thermal analysis

DTA measurements were carried out using a calibrated LABSYS Evo TG–DTA thermal analyser with α-Al_2O_3 used as the inert reference material. A 40 mg coupon of the as-prepared wire was loaded into a platinum (Pt) crucible with Al_2O_3 as the reference material and scanned from room temperature to 400 °C under flowing inert atmosphere. Five constant heating rates were employed: β = 10, 15, 20, 25 and 30 °C min^{-1}. Temperature and heat-flow calibration were performed using high-purity indium (T_m = 156.6 °C) and tin (Tm = 231.9 °C) standards, consistent with the fixed points tabulated in the NIST solder-properties database [1] and in Smithells [25]. A freshly prepared coupon was used at each heating rate to minimise oxidation effects. The instrument calibration at each heating rate provides the heating-rate-dependent thermal-lag correction applied to all reported temperatures. The corrected onset temperatures confirm that the residual thermal lag across the β = 10–30 °C min^{-1} range is substantially smaller than the 14.2 °C shift observed in peak temperature Tp, such that the kinetic fits are not materially affected by uncorrected lag.

3.3. Peak parameter extraction and kinetic analysis

Onset (T_0), peak (T_p), and end (T_{end}) temperatures were extracted from each thermogram by the conventional tangent-baseline construction. The peak area, reported by the instrument in μV·s mg^{-1}, is proportional to the enthalpy of the transformation through the instrument calibration constant. Activation energies were derived from eqs. (3), (4), and (5) by linear regression of the appropriate transformed quantities against $1000/T_p$ (in K^{-1}).

4. Results and discussion

4.1 Differential thermal analysis (DTA) of Pb-61.9Sn-2Al

DTA scans at all five heating rates exhibited a single well-defined thermal event within the 25–400 °C range (Figure 1): the principal endothermic eutectic Pb–Sn melting transformation, characterised by a sharp, deep endotherm with onset near 184 °C and a heating-rate-dependent peak position in the 195–210 °C range. The transients observed at the low-temperature start of each curve (β = 15, 20, 25 and 30 °C min^{-1}) correspond to instrument equilibration and were excluded from the kinetic analysis. A minor exothermic feature at ~380–390 °C, common to all five scans and of sub-microvolt amplitude (<10% of the main endotherm), is attributed to surface oxidation of the molten Sn-rich phase by residual oxygen in the purge gas a documented oxidation behaviour of liquid Sn-rich solders, including eutectic Pb–Sn, in this temperature range [28], and is unrelated to any equilibrium transformation in the Pb–Sn–Al system. No other thermal events were resolved up to 400 °C, indicating that the 2 wt% Al microaddition introduces no detectable melting endotherm of an Al-rich

phase within this interval, consistent with the very low solid solubility of Al in both Pb and Sn [2,25] and the absence of stable low-temperature Al-containing intermetallics in the Pb-Sn-Al system.

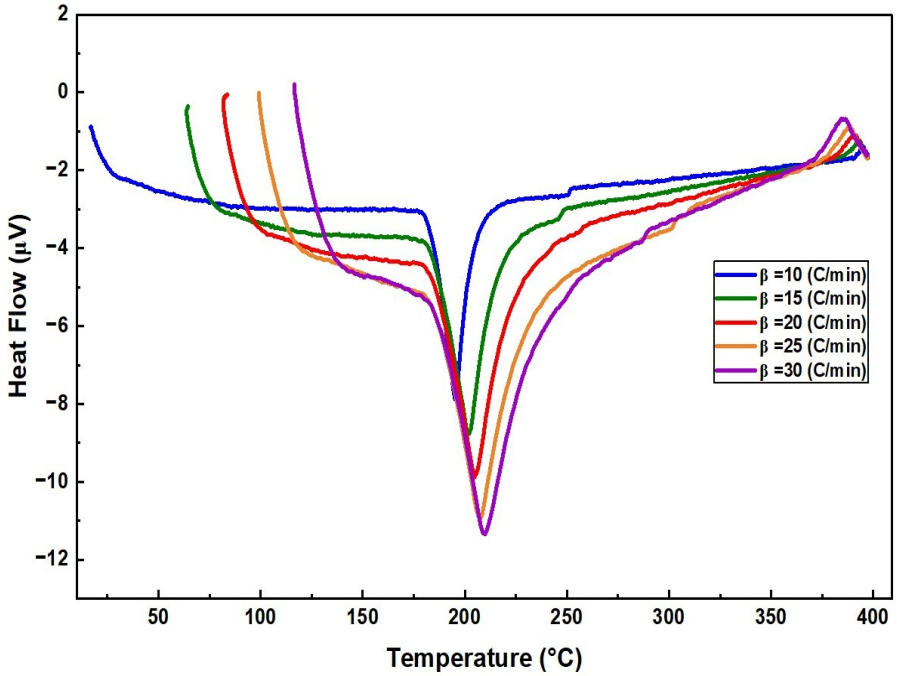


Figure 1. DTA thermograms of Pb–61.9Sn–2Al at five constant heating rates

4.2. Characteristic temperatures and enthalpy of fusion

The peak temperature T_p shifted systematically from 195.35 °C at β = 10 °C min^{-1} to 209.55 °C at β = 30 °C min^{-1} (Table 1), and the onset T0 increased from 184.49 to 190.85 °C, remaining within +1.5 to +7.9 °C of the canonical Pb-Sn eutectic of 183 °C tabulated in the NIST solder-properties database [1] and in the DSC study of Pb-Sn solid/liquid transformation data by Pedersen et al. [26]. The small positive offset at the lowest β is attributable to the 2 wt% Al microaddition combined with thermal lag; at higher heating rates the onset shift is dominated by the kinetic broadening of the transformation. The total T_p shift of 14.20 °C is an exceptionally clean kinetic observable that supports the application of the methods of Kissinger [11], Ozawa–Flynn–Wall [12,13] and Augis–Bennett [14] to extract the apparent activation energy.

Table 1. Experimental peak parameters of Pb-61.9Sn-2Al alloy melting endotherm.

β (°C min^{-1})	T_o (°C)	T_p (°C)	T_{end} (°C)	$T_{end} - T_o$ (°C)	Heat (μV·s mg^{-1})
10	184.49	195.35	202.53	18.04	8.233
15	186.66	201.80	211.92	25.26	7.609
20	188.51	204.85	218.27	29.76	6.858
25	189.29	207.40	237.36	48.07	7.052
30	190.85	209.55	241.52	50.67	6.818

Figure 2 illustrates the heating-rate dependence of the eutectic melting behaviour of the Pb-61.9Sn-2Al alloy. Figure 2(a) plots the three characteristic temperatures onset (T_{onset}, green squares), peak (T_p,

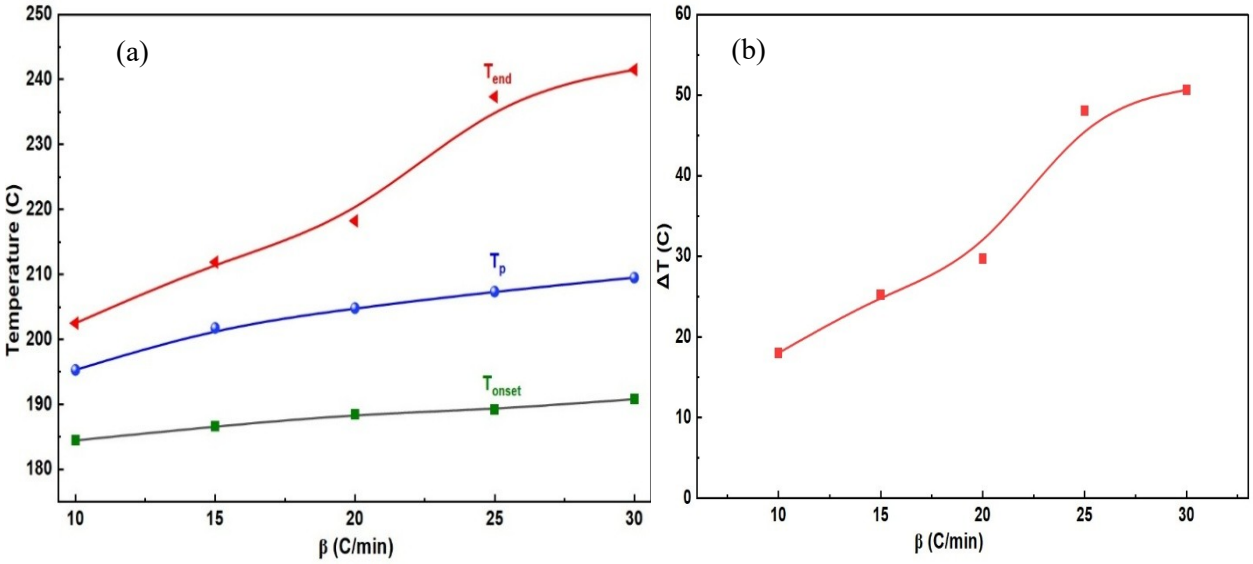


Figure 2. Heating-rate dependence of (a) characteristic temperatures of the alloy melting endotherm ; and (b) peak broadening ΔT of the Pb-61.9Sn-2Al alloy

blue diamonds) and end (T_{end}, red triangles) as a function of heating rate β. All three temperatures increase monotonically with β: T_{onset} rises gently from 184.49 °C at β = 10 °C min^{-1} to 190.85 °C at β = 30 °C min^{-1} (a modest +6.4 °C shift), T_p shifts by +14.20 °C across the same interval, while T_{end} exhibits the steepest dependence, climbing from 202.53 °C to 241.52 °C (+39 °C). The widening vertical spread between the three curves with increasing β provides direct visual evidence of kinetic broadening of the transformation. Figure 2(b) shows the corresponding peak width $\Delta T = T_{end} - T_{onset}$ as a function of β; ΔT increases monotonically from 18.0 °C at β = 10 °C min^{-1} to 50.7 °C at β = 30 °C min^{-1} almost a threefold broadening across the experimental range with the steepest rise occurring between β = 20 and 25 °C min^{-1}. The peak width $T_{end} - T_0$ broadens monotonically from 18.04 °C to 50.67 °C as β increases from 10 to 30 °C min^{-1}, almost a threefold increase. By comparison, pure Sn-37Pb eutectic typically exhibits a peak width below 10 °C at comparable heating rates [3,26,27].

4.3 Kissinger analysis

Application of the Kissinger formulation, eq. (3), to the peak temperatures of Table 1 gives the transformed quantities summarised in Table 2.

Table 2. Kissinger transformation of the Pb-61.9Sn-2Al alloy melting peak data.

β (°C min⁻¹)	T_p (K)	1000/T_p (K^{-1})	T_p^2 (K^2)	ln(β/T_p^2)
10	468.50	2.1345	219492.2	−14.089
15	474.95	2.1055	225577.5	−13.712
20	478.00	2.0921	228484.0	−13.437
25	480.55	2.0810	230928.3	−13.225
30	482.70	2.0717	233000.3	−13.052

Linear regression of these data, shown in Figure 3, gives a slope of −16.674 K and an intercept of 21.461, with a coefficient of determination $R^2 = 0.989$. The apparent activation energy, $E_a = -\text{slope} \times R$, is 138.63 kJ mol^{-1}. The pre-exponential factor estimated from the Kissinger intercept is $A \approx 3.5 \times 10^{13}$ s^{-1}, for a melting transition this parameter serves as a formal regression coefficient extracted from the Kissinger intercept rather than a physical attempt frequency, and its absolute value is not independently interpreted here [21,24].

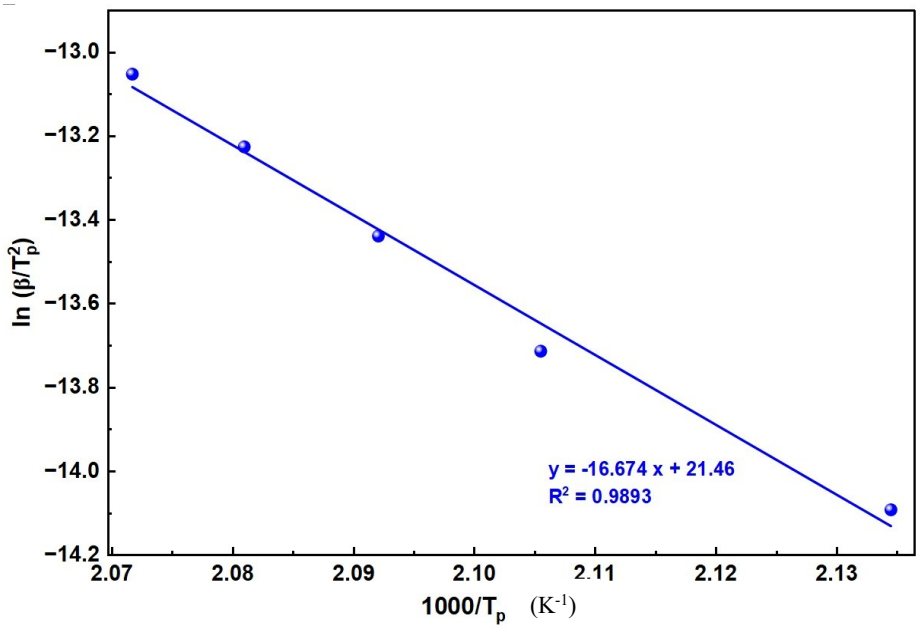


Figure 3 Kissinger plot, ln(β/T_p^2) vs 1000/T_p of the Pb-61.9Sn-2Al alloy

4.4. Ozawa-Flynn-Wall analysis

The model-free integral treatment was applied via eq. (4), with the corresponding regression shown in Figure 4. Linear regression of log10 β on 1000/T_p produced a slope of −7.654 K and an intercept of 17.321, with R^2 = 0.990. The corresponding apparent activation energy is 139.35 kJ mol^{-1}.

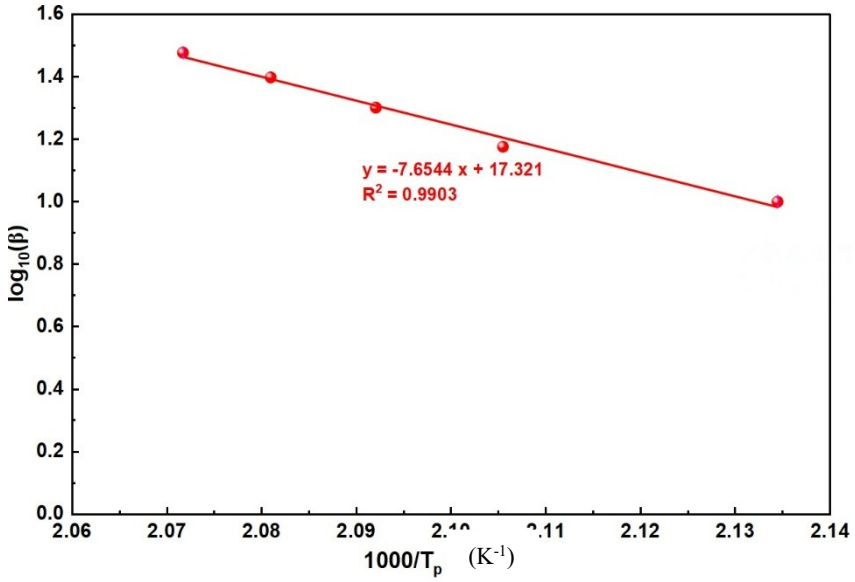


Figure 4 Ozawa–Flynn–Wall plot, $\log_{10}(\beta)$ vs 1000/T_p of the Pb-61.9Sn-2Al alloy

The relative deviation between this value and the Kissinger estimate is less than 0.5 %. Because the Kissinger and OFW expressions are near-identical transforms of the same (β, T_p) dataset, however, this close agreement is expected by construction; it therefore represents internal arithmetic consistency in the application of the two model-free treatments, and not an independent, method-independent cross-validation of the absolute value of E_a [24].

4.5. Augis-Bennett analysis

Application of the Augis-Bennett expression, eq. (5), incorporates the onset temperature T_0 through the temperature interval ($T_p - T_0$). The corresponding plot is shown in Figure 5 linear regression yields a slope of −8.856 K and an intercept of 14.657, with R^2 = 0.891. The corresponding apparent activation energy is 73.63 kJ mol^{-1}. The systematic reduction of E_a relative to the Kissinger and OFW estimates is a known consequence of the Augis-Bennett formulation: by normalising the heating rate by the temperature interval ($T_p - T_0$), which is itself an increasing function of β (Table 1; Figure 2b), the method partially absorbs the kinetic broadening into the apparent activation energy. The lower R^2 for this method (0.891 vs 0.989) reflects the noise introduced by this normalisation when ($T_p - T_0$) varies

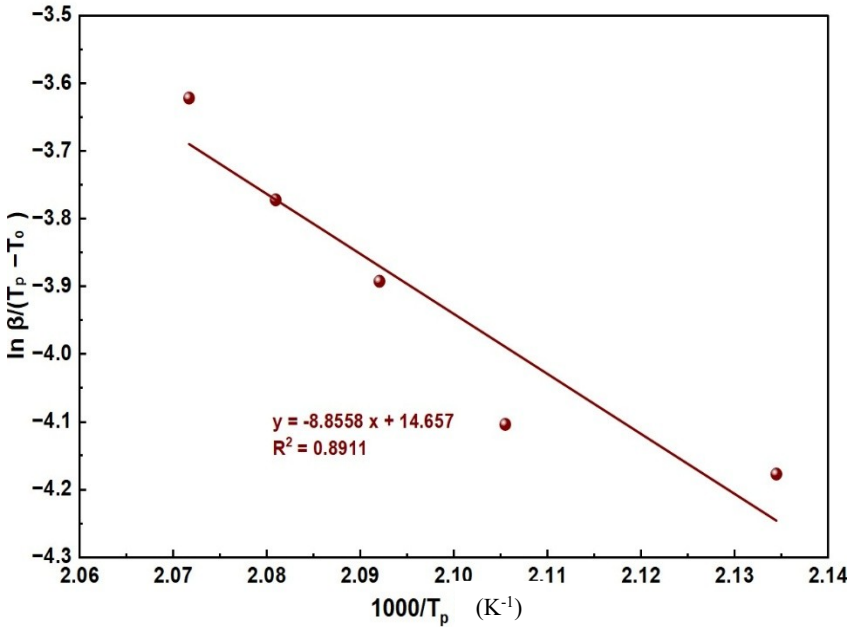


Figure 5. Augis–Bennett plot , $\ln[\beta/(T_p - T_0)]$ vs $1000/T_p$ of the Pb-61.9Sn-2Al alloy

strongly with β. Similar systematic discrepancies between Augis-Bennett and Kissinger estimates have been reported for crystallisation of chalcogenide glasses and amorphous metallic alloys [19,29].

4.6. Comparative kinetic assessment

Table 3 summarises the regression statistics and apparent activation energies obtained from the three methods, and Figure 6 compares the three values graphically against the established literature range for Pb–Sn solder melting kinetics. The Kissinger–OFW pair converge to $E_{a,app} \approx 139$ kJ mol^{-1} and are reported as the primary kinetic descriptor for this system. This figure lies firmly within the range of 50–200 kJ mol^{-1} reported for melting kinetics of low-melting Sn-based metallic alloys [26,29,30]. The systematic offset of the Augis–Bennett value reflects the genuine kinetic broadening of the peak with heating rate, an observable physical phenomenon rather than a defect of the method, and is therefore retained in the kinetic record as an independent indicator of microstructure-mediated heat transport in the alloy.

Table 3. Apparent activation energies from the three non-isothermal methods applied to the Pb-61.9Sn-2Al alloy melting peak.

Method	Slope (K)	Intercept	R^2	E_a (kJ mol^{-1})
Kissinger	−16.674	21.461	0.989	138.63
Ozawa-Flynn-Wall	−7.654	17.321	0.990	139.35
Augis-Bennett	−8.856	14.657	0.891	73.63

Figure 6 compares the apparent activation energy E_a of the eutectic Pb–Sn melting peak obtained from the three non-isothermal methods. The Kissinger and Ozawa–Flynn–Wall bars (138.6 and 139.3 kJ mol^{-1}) are visually indistinguishable, reflecting the ~0.5 % mutual deviation between the two model-free treatments and confirming the robustness of the kinetic descriptor. The Augis–Bennett bar (73.6 kJ mol^{-1}) is systematically displaced downward, a consequence of its normalisation by the heating-rate-dependent interval ($T_p - T_0$). All three values lie firmly within the green-shaded literature range of 50–200 kJ mol^{-1} reported for melting kinetics of low-melting Sn-based solder alloys; the dotted horizontal line marks the arithmetic mean across the three estimates (117.2 kJ mol^{-1}), shown for reference only and not regarded as a physical descriptor; see Section 4.6) and the regression quality of each method is inscribed within the corresponding bar (R^2 = 0.989, 0.990 and 0.891 for Kissinger, OFW and Augis–Bennett, respectively).

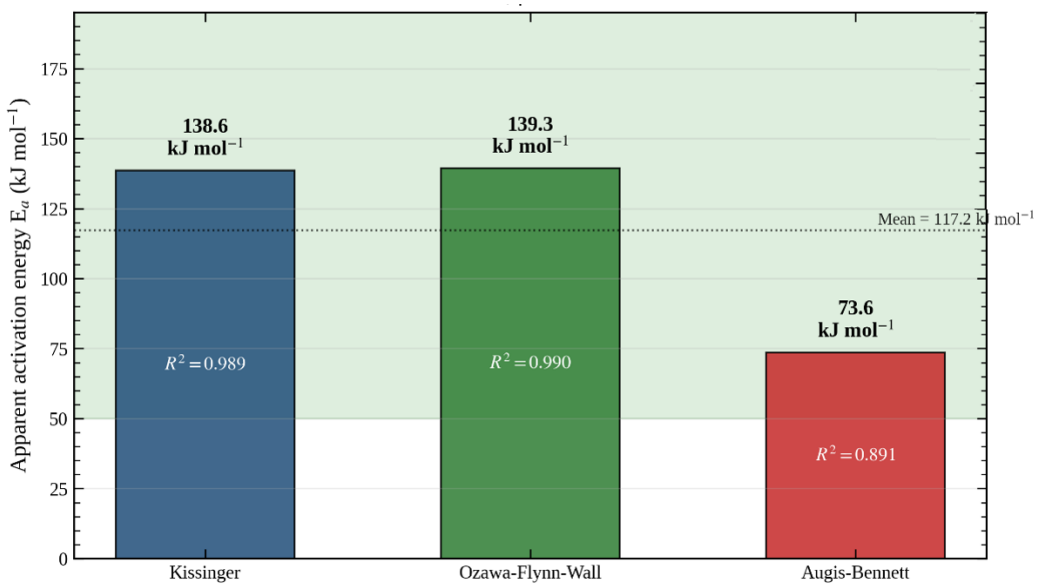


Figure 6. Apparent activation energy E_a for the melting peak in Pb-61.9Sn-2Al obtained from the three non-isothermal methods

4.7. Role of the aluminium microaddition

The persistence of a single, well-defined endothermic event with onset near 183 °C across all heating rates (Figure 1, Figure 2a) demonstrates that the eutectic Pb-Sn melting transformation is preserved in the presence of 2 wt% Al. The Al microaddition, however, produces a striking broadening of the melting peak: the total peak width ($T_{end} - T_0$) increases from 18.04 °C at β = 10 °C min^{-1} to 50.67 °C at β = 30 °C min^{-1} (Table 1; Figure 2b). In binary Sn-37Pb eutectic the corresponding width is typically below 10 °C at comparable heating rates [3,26,27]. The DTA data for the binary Pb–61.9Sn reference

alloy prepared alongside the ternary (Section 3.1) are available in Ref. [8].These dispersoids do not participate in the eutectic transformation, but they reduce the volume fraction of the eutectic phase available for melting at any given temperature and impose a fine-scale partitioning of the heat flow during the transformation, which manifests in DTA as peak broadening. This interpretation is consistent with the established role of insoluble dispersoids in metallic systems [27,29,31]. From a process-engineering standpoint, the practical implication is that the recommended reflow window for an Al-modified Pb-Sn solder must be widened relative to the binary eutectic to ensure complete melting throughout the joint volume. Using the highest peak temperature observed in the present study (T_p = 209.55 °C at β = 30 °C min^{-1}) and adding the customary 20–30 °C process margin recommended for Pb-Sn reflow [4,6,7], a peak reflow temperature of 230–240 °C would be appropriate for the Pb-61.9Sn-2Al formulation. This value remains comfortably below the upper bound of conventional reflow profiles and is therefore fully compatible with existing surface-mount infrastructure.

5. Conclusions

The non-isothermal thermal signature of a Pb–61.9Sn–2Al alloy has been characterised by DTA at five heating rates using a 40 mg specimen. The principal findings are:

- A single, well-defined endothermic transformation was resolved in every thermogram, corresponding to the eutectic Pb–Sn melting event, whose peak temperature shifted systematically from 195.35 °C to 209.55 °C across β = 10–30 °C min^{-1}.
- The melting onset (184.5–190.9 °C) confirms preservation of the canonical Pb –Sn eutectic; the 2 wt% Al microaddition does not displace the eutectic temperature.
- Kissinger and Ozawa–Flynn–Wall analyses converge to E_a = 138.63 and 139.35 kJ mol^{-1} ($R^2 \geq 0.989$; ~0.5 % mutual deviation), which represents internal arithmetic consistency between two near-identical transforms of the same (β, T_p) data rather than independent cross-validation; the Kissinger/OFW value (≈139 kJ mol^{-1}) is therefore adopted as the base apparent-activation-energy indicator. Augis–Bennett returns the lower 73.63 kJ mol^{-1} (R^2 = 0.891), reflecting its sensitivity to the heating-rate-dependent peak width.
- The 2 wt% Al microaddition broadens the melting peak nearly threefold while leaving the eutectic onset unshifted, reflecting the diagnostic thermal signature of dispersed insoluble Al-rich grains in the Pb-Sn matrix.

These results provide quantitative kinetic and thermophysical descriptors for a previously under-characterised Pb–Sn–Al solder composition and establish a baseline for the systematic compositional optimisation of Al-modified tin–lead solders with potential relevance to electronic joining applications.

References

[1] Siewert T, Liu S, Smith DR, Madeni JC. Database for Solder Properties with Emphasis on New Lead-free Solders, Release 4.0. Boulder (CO): NIST and Colorado School of Mines; 2002. Available at: https://www.nist.gov/publications/database-solder-properties-emphasis-new-lead-free-solders

[2] Massalski TB, editor. Binary Alloy Phase Diagrams. 2nd ed. Materials Park (OH): ASM International; 1990. ISBN 978-0871704030.

[3] Glazer J. Microstructure and mechanical properties of Pb-free solder alloys for low-cost electronic assembly: a review. J Electron Mater. 1994;23(8):693–700. https://doi.org/10.1007/BF02651361

[4] Abtew M, Selvaduray G. Lead-free solders in microelectronics. Mater Sci Eng R Rep. 2000;27(5–6):95–141. https://doi.org/10.1016/S0927-796X(00)00010-3

[5] Suganuma K. Advances in lead-free electronics soldering. Curr Opin Solid State Mater Sci. 2001;5(1):55–64. https://doi.org/10.1016/S1359-0286(00)00036-X

[6] Manko HH. Solders and Soldering: Materials, Design, Production, and Analysis for Reliable Bonding. 4th ed. New York: McGraw-Hill; 2001. ISBN 978-0071341394.

[7] Hwang JS. Modern Solder Technology for Competitive Electronics Manufacturing. New York: McGraw-Hill; 1996. ISBN 978-0070317499.

[8] Alnakhlani A, Hassan B, Abdulhafiz M. Effect of Al addition on the thermal properties of lead–tin alloy. Results Mater. 2021;12:100229. https://doi.org/10.1016/j.rinma.2021.100229

[9] Frear DR, Burchett SN, Morgan HS, Lau JH, editors. The Mechanics of Solder Alloy Interconnects. New York: Van Nostrand Reinhold; 1994. ISBN 978-0442012007.

[10] Vianco PT. General soldering. In: ASM Handbook, Vol. 6: Welding, Brazing, and Soldering. Materials Park (OH): ASM International; 1993. p. 938–58. ISBN 978-0871703828.

[11] Kissinger HE. Reaction kinetics in differential thermal analysis. Anal Chem. 1957;29(11):1702–6. https://doi.org/10.1021/ac60131a045

[12] Ozawa T. A new method of analyzing thermogravimetric data. Bull Chem Soc Jpn. 1965;38(11):1881–6. https://doi.org/10.1246/bcsj.38.1881

[13] Flynn JH, Wall LA. A quick, direct method for the determination of activation energy from thermogravimetric data. J Polym Sci B Polym Lett. 1966;4(5):323–8. https://doi.org/10.1002/pol.1966.110040504

[14] Augis JA, Bennett JE. Calculation of the Avrami parameters for heterogeneous solid state reactions using a modification of the Kissinger method. J Therm Anal. 1978;13(2):283–92. https://doi.org/10.1007/BF01912301

[15] Avrami M. Kinetics of phase change. I. General theory. J Chem Phys. 1939;7(12):1103–12. https://doi.org/10.1063/1.1750380

[16] Friedman HL. Kinetics of thermal degradation of char-forming plastics from thermogravimetry. Application to a phenolic plastic. J Polym Sci C Polym Symp. 1964;6(1):183–95. https://doi.org/10.1002/polc.5070060121

[17] Šesták J, Berggren G. Study of the kinetics of the mechanism of solid-state reactions at increasing temperatures. Thermochim Acta. 1971;3(1):1–12. https://doi.org/10.1016/0040-6031(71)85051-7

[18] Doyle CD. Estimating isothermal life from thermogravimetric data. J Appl Polym Sci. 1962;6(24):639–42. https://doi.org/10.1002/app.1962.070062406

[19] Boswell PG. On the calculation of activation energies using a modified Kissinger method. J Therm Anal. 1980;18(2):353–8. https://doi.org/10.1007/BF02055820

[20] Matusita K, Sakka S. Kinetic study of crystallization of glass by differential thermal analysis—criterion on application of Kissinger plot. J Non-Cryst Solids. 1980;38–39(2):741–6. https://doi.org/10.1016/0022-3093(80)90525-6

[21] Vyazovkin S, Burnham AK, Criado JM, Pérez-Maqueda LA, Popescu C, Sbirrazzuoli N. ICTAC Kinetics Committee recommendations for performing kinetic computations on thermal analysis data. Thermochim Acta. 2011;520(1–2):1–19. https://doi.org/10.1016/j.tca.2011.03.034

[22] Vyazovkin S, Chrissafis K, Di Lorenzo ML, Koga N, Pijolat M, Roduit B, Sbirrazzuoli N, Suñol JJ. ICTAC Kinetics Committee recommendations for collecting experimental thermal analysis data for kinetic computations. Thermochim Acta. 2014;590:1–23. https://doi.org/10.1016/j.tca.2014.05.036

[23] Starink MJ. The determination of activation energy from linear heating rate experiments: a comparison of the accuracy of isoconversion methods. Thermochim Acta. 2003;404(1–2):163–76. https://doi.org/10.1016/S0040-6031(03)00144-8

[24] Vyazovkin S. Kissinger method in kinetics of materials: things to beware and be aware of. Molecules. 2020;25(12):2813. https://doi.org/10.3390/molecules25122813

[25] Brandes EA, Brook GB, editors. Smithells Metals Reference Book. 7th ed. Oxford: Butterworth-Heinemann; 1992. ISBN 978-0750610209.

[26] Pedersen AS, Pryds N, Linderoth S, Larsen PH, Kjøller J. The determination of dynamic and equilibrium solid/liquid transformation data for Pb-Sn using DSC. J Therm Anal Calorim. 2001;64(3):887–94. https://doi.org/10.1023/A:1011506526074

[27] Lee NC. Reflow Soldering Processes and Troubleshooting: SMT, BGA, CSP and Flip Chip Technologies. Boston (MA): Newnes; 2002. ISBN 978-0750672184.

[28] Lin KL, Liu TP. High-temperature oxidation of a Sn-Zn-Al solder. Oxid Met. 1998;50(3–4):255–67. https://doi.org/10.1023/A:1018840405283

[29] Mehta N, Kumar A. Comparative analysis of calorimetric studies on Se85Te10M5 (M = Ag, Zn and Cd) chalcogenide glasses. J Therm Anal Calorim. 2007;87(2):343–9. https://doi.org/10.1007/s10973-006-7720-1

[30] Mavoori H, Chin J, Vaynman S, Moran B, Keer L, Fine M. Creep, stress relaxation, and plastic deformation in Sn-Ag and Sn-Zn eutectic solders. J Electron Mater. 1997;26:783–90. https://doi.org/10.1007/s11664-997-0252-z

[31] McCabe RJ, Fine ME. Athermal and thermally activated plastic flow in low melting temperature solders at small stresses. Scr Mater. 1998;39(2):189–95. https://doi.org/10.1016/S1359-6462(98)00149-4